Available online at www.sciencedirect.com
SCIENCE DIRECT®
International Journal of Heat and Fluid Flow 24 (2003) 54–66
International Journal of HEAT AND FLUID FLOW
www.elsevier.com/locate/ijhff

Three-dimensional study of flow past a square cylinder at low Reynolds numbers

A.K. Saha, G. Biswas *, K. Muralidhar

Department of Mechanical Engineering, Indian Institute of Technology, Kanpur, 208 016 UP, India

Received 7 December 2001; accepted 30 July 2002

Abstract

The spatial evolution of vortices and transition to three-dimensionality in the wake of a square cylinder have been numerically studied. A Reynolds number range between 150 and 500 has been considered. Starting from the two-dimensional Kármán vortex street, the transition to three-dimensionality is found to take place at a Reynolds number between 150 and 175. The three-dimensional wake of the square cylinder has been characterized using indicators appropriate for the wake of a bluff body as described by the earlier workers. In these terms, the secondary vortices of Mode-A are seen to persist over the Reynolds number range of 175–240. At about a Reynolds number of 250, Mode-B secondary vortices are present, these having predominantly small-scale structures. The transitional flow around a square cylinder exhibits an intermittent low frequency modulation due to the formation of a large-scale irregularity in the near-wake, called vortex dislocation. The superposition of vortex dislocation and the Mode-A vortices leads to a new pattern, labelled as Mode-A with dislocations. The results for the square cylinder are in good accordance with the three-dimensional modes of transition that are well-known in the circular cylinder wake. In the case of a circular cylinder, the transition from periodic vortex shedding to Mode-A is characterized by a discontinuity in the Strouhal number–Reynolds number relationship at about a Reynolds of 190. The transition from Mode-A to Mode-B is characterized by a second discontinuity in the frequency law at a Reynolds number of ≈250. The numerical computations of the present study with a square cylinder show that the values of the Strouhal number and the time-averaged drag-coefficient are closely associated with each other over the range of Reynolds numbers of interest and reflect the spatial structure of the wake.

Keywords: Square cylinder; Vorticity; Vortex shedding; Vortex dislocation; Strouhal number; Secondary vortices

1. Introduction

Unsteady flow around bluff bodies is a topic of practical importance. For example, the accurate estimation of the vortex shedding frequency is required for the design of structures exposed to fluid flow. The vortex shedding frequency and more generally the wake behavior depend on different aspects of the flow field such as the end conditions, blockage ratio of the flow passage, upstream turbulence level and the aspect ratio of the bluff body. Cylinders with circular and the square cross-sections have been adopted in the previous studies as shapes whose wakes can be analyzed to evolve a fundamental understanding of the dynamics involved. Between the two, the circular geometry has received considerable attention. To extend the study further, the square cylinder forms the subject of analysis in the present work.

Okajima (1982) has conducted an extensive experimental study for the rectangular bluff body configuration over a Reynolds numbers range of 100 and 2×10^4 in an unbounded medium. Here the Reynolds number (Re) is defined as $u_{av}B/v$ in terms of the average incoming velocity, the obstacle width and the kinematic viscosity. For a square cylinder, the Strouhal number, S ($= fB/u_{av}$, with f as the frequency of vortex shedding, in Hz) was found to vary slightly yet continuously around a value of 0.13. Davis et al. (1984) have compared their numerical and experimental results for flow around a rectangular cylinder in a horizontal channel with Reynolds number ranging from 100 to 2000. The numerical prediction was found to agree well with the experiments.

* Corresponding author. Tel.: +91-512-597616; fax: +91-512-597408.
E-mail address: gtm@iitk.ac.in (G. Biswas).

0142-727X/02/$ - see front matter © 2002 Elsevier Science Inc. All rights reserved.
PII: S0142-727X(02)00208-4

Tombazis and Bearman (1997) have shown that above a critical Reynolds number, vortex shedding from nominally two-dimensional bluff bodies reveals three-dimensional behavior. They also suggest that the three-dimensionality can be characterized by the spanwise correlation length (in terms of diameters of the bluff body) of fluctuating velocity in the wake or fluctuating pressure on the body surface. The recent development in understanding flow past bluff bodies, especially the flow past a circular cylinder has been discussed in the review paper Williamson (1996a).

The structure of the wake behind a circular cylinder at a low Reynolds number is characterized by a staggered array of vortices. The two-dimensionality of vortex shedding is preserved in the Reynolds number range of 45–180, but is sensitive to end conditions. A recent discovery which sheds light on the major reason for three-dimensionality in nominally two-dimensional geometries is vortex dislocation (Williamson, 1989, 1992).

Recent work in the low Reynolds number range for a circular cylinder indicate that the transition from periodic vortex shedding to Mode-A is characterized by a discontinuity is *S–Re* relationship at about a Reynolds number of 190. The wake undergoes a transition to a less ordered state followed by the formation of the secondary spatial structures having different spanwise wavelengths. Williamson (1996b) has reported dominant scales having wavelength of 3.0–4.0 cylinder diameters. The transition from Mode-A to Mode-B is characterized by a second discontinuity in the frequency law. Mode-B is observed around a Reynolds number of 250 with dominant spanwise wavelength of one cylinder diameter. Williamson (1992, 1996b,c) has observed the presence of large-scale low frequency structures in the transition process during the presence of Mode-A. These are called vortex dislocations. The visualizations of Williamson reveal that Mode-A represents the inception of streamwise vortex loops and large-scale vortex dislocations. Mode-B entails more coherent vortex shedding, with superimposed small-scale perturbations.

Mittal and Balachandar (1995) have reported direct numerical simulation for a circular cylinder in the transitional regime. They show that the streamwise secondary structures are formed as a consequence of stretching of the core vorticity. A time domain analysis of transition to chaos in the wake of a square cylinder has been reported by the authors elsewhere (Saha et al., 2000a). In a related study, the authors have explored the similarity between the instantaneous wake pattern of a square cylinder at low Reynolds number with the phase-averaged turbulent flow fields at very high Reynolds number (Saha et al., 2000b).

Two recent studies focus on the transition in the low Reynolds number wake of a square cylinder (Robichaux et al., 1999; Sohankar et al., 1999). Sohankar et al. (1999) have carried out an analysis using a finite volume DNS in two and three-dimensions. The vortex structures similar to Mode-A wake instability of circular cylinder flow, have been identified by them. The spanwise wavelengths of such instabilities vary between 2 and 4 diameters. For $Re \geqslant 250$, they have observed the vortex structures similar to Mode-B wake instability with a dominant wavelength of about one diameter.

Three-dimensional instabilities in a two-dimensional periodic wake have been investigated by Robichaux et al. (1999) using Floquet stability analysis. They have found Mode-A instability at a Reynolds number of 162, followed by a short wavelength (Mode-B) instability at a Reynolds number of about 190. In addition, they have observed another intermediate transition mode which they call as Mode-S instability. Mode-S has a spanwise wavelength of 2.8 diameters and this mode occurs at around $Re = 200$.

The present work is aimed at the numerical simulation of the flow past a square cylinder for Reynolds numbers in the range 125–500. The simulation is intended to clarify the transition scenario of the wake of a square cylinder. Emphasis is placed on the appearance of three-dimensional phenomena in the transitional flow regime. The three-dimensional phenomena encountered in the present work are shedding dominated but involve Mode-A and Mode-B patterns as well as vortex dislocation. The time-averaged and the fluctuating field have been analyzed to examine the integral parameters such as lift and drag-coefficients and the Strouhal number. In this respect, the present study supplements the semi-analytical and DNS research on the low Reynolds number wake of a square cylinder.

2. Governing equations and boundary conditions

The unsteady, three-dimensional Navier–Stokes equations along with the incompressibility constraint have been numerically solved in the present study. The equations for continuity and momentum in dimensionless form may be expressed as

$$\frac{\partial u_i}{\partial x_i} = 0 \tag{1}$$

$$\frac{\partial u_i}{\partial t} + \frac{\partial (u_j u_i)}{\partial x_j} = -\frac{\partial p}{\partial x_i} + \frac{1}{Re}\frac{\partial^2 u_i}{\partial x_j^2} \tag{2}$$

In the above equations the velocities are nondimensionalized with the average velocity u_{av}, all lengths with the obstacle width B and pressure by ρu_{av}^2.

The geometry and the relevant dimensions considered for analysis are schematically shown in Fig. 1. The dimensions related to the geometry in the figure are $B = 1.0$, $L_a = 6.0$, $L = 24.0$, $H = 10.0$ and $A = 6.0$. To show the effect of aspect ratio on flow structures, calculations have also been done using $A = 10$. In relation to this

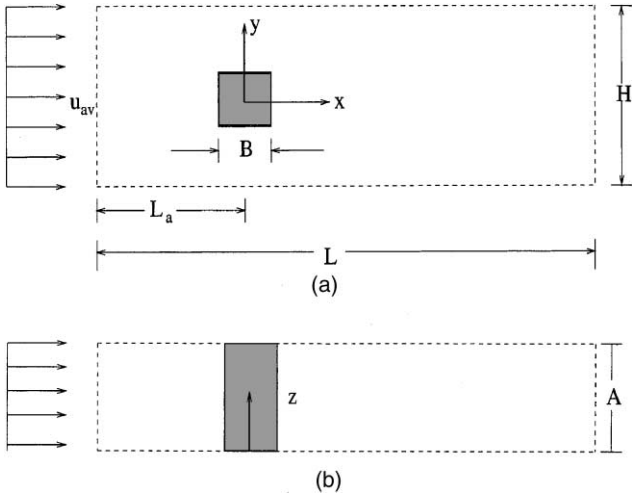

Fig. 1. Model of flow past a square cylinder: (a) top view, (b) side view.

figure, the boundary conditions employed for the present investigation are: (i) The confining surfaces are modeled as the free-slip; for example, at the transverse confining surfaces $y = \pm H/2$, $\partial u/\partial y = v = \partial w/\partial y = 0$ (ii) At the inlet, a constant streamwise velocity has been used with other velocities being set to zero (iii) There is no unique prescription for the outflow plane. The idea is to have the conditions which do not affect the flow in the upstream. To this end, the following boundary condition has been used (Orlanski, 1976)

$$\frac{\partial u_i}{\partial t} + u_c \frac{\partial u_i}{\partial x} = 0 \tag{3}$$

where u_c, the convective velocity is the celerity (Saha et al., 2000b) of vortices leaving the outflow plane. For all the solid surfaces on the obstacle, the no-slip boundary condition ($u = v = w = 0$) has been used.

3. Method of solution

The differential equations (1) and (2) have been solved on a staggered grid by the MAC algorithm of Harlow and Welch (1965), as modified by Hoffman and Benocci (1994). In the present study, advection and diffusion terms have both been approximated by the central differencing scheme. Fine grids have been used in the present simulation. Hence it was possible to eliminate spurious oscillations associated with the central differencing of the advection terms, while keeping the truncation errors within limits. Special attention has been laid on the local order of accuracy as well as the global energy conserving properties of the numerical solution. The Adams–Bashforth scheme having second order accuracy in time, has been used for time advancement. The Courant–Friedrichs–Lewy condition and Fourier stability condition were used to determine the time step. The final time step was less than the minimum of the above two. A typical value of the time step for three-dimensional computation in the Reynolds number range of 325 is 0.015. The data used in this investigation are necessarily free from the bias of the initial transients. The details of the numerical scheme have been presented by the authors elsewhere (Saha, 1999).

For computation, the flow domain is divided into a number of hexahedral cells. The mesh is nonuniform on the x–y plane but uniform on all x–z planes. The grid is clustered near the cylinder and the spacing is increased in a proper ratio away from the cylinder. The grid on which results have been obtained has $178 \times 80 \times 22$ cells in the x, y and z directions. Grid independence tests were accomplished satisfactorily using three other grid-meshes, such as, $178 \times 80 \times 32$, $214 \times 104 \times 22$ and $178 \times 80 \times 42$.

All the computations have been carried out in a 233 MHz and 256 MB RAM DEC-ALPHA workstation. The typical CPU time per time step at the dynamic steady state condition taken on $178 \times 80 \times 22$ grid at a Reynolds number of 500 is about 15 min.

4. Results and discussion

Studies with a circular as well as the square cylinder show that transition to three-dimensionality can occur at a low Reynolds number even when the overall configuration is two-dimensional. The associated critical Reynolds number is expected to depend on factors such as the inlet disturbance level, the shape of the body and the velocity profile in the approach flow.

In the present study for a square cylinder, upstream disturbances are absent and transition is promoted by discretization errors arising from the governing equations along with those from the boundary conditions. These are being uniformly distributed over the fluid region, and the transition observed in the present computations can be thought of as being natural, rather than forced. The corresponding critical Reynolds number can be regarded as the upper limit for transition.

Fig. 2(a) exhibits the signal traces of the spanwise component of velocity in the near-wake at Reynolds numbers of 150 and 175. With the passage of time the velocity component at $Re = 150$ goes to zero indicating that the flow is two-dimensional. At a Reynolds number of 175, intermittent fluctuations are seen even at longer times. The amplitude of fluctuations in the spanwise velocity increases with increasing Reynolds number. Simultaneously there is a decrease in the intermittency of the fluctuations. The intermittency fades out at a Reynolds number of 250. Beyond, low frequency fluctuations are not present and the signal trace is uniformly noisy. Fig. 2(b) depicts the time variation of the spanwise velocity at a Reynolds number of 325.

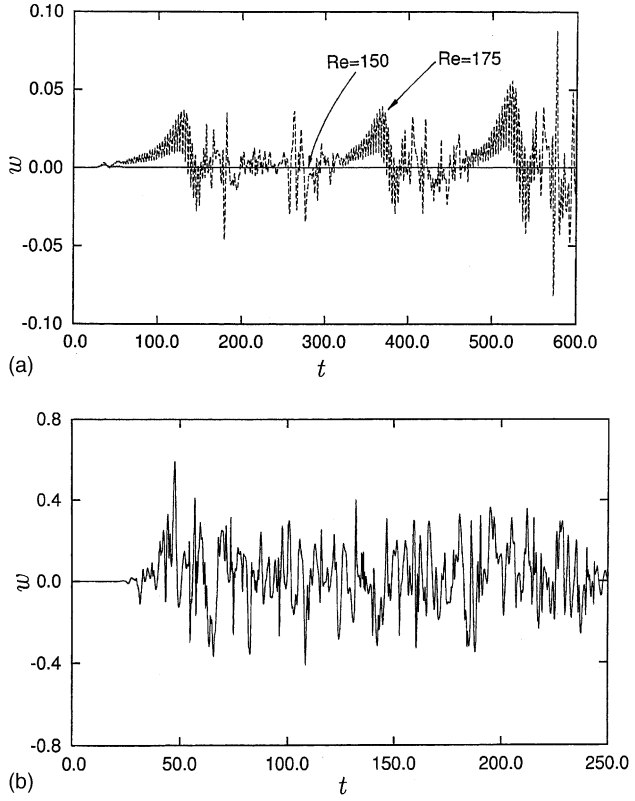

Fig. 2. Time traces of the spanwise component of velocity: (a) $Re = 150$ and 175 and (b) $Re = 325$ at $x = 1.7$, $y = 0$ and $z = 3$.

The signals in Fig. 2(a) and (b) are a clear indication of transition to three-dimensionality in the wake of the square cylinder. The critical Reynolds number can be taken to lie between 150 and 175. Robichaux et al. (1999) have performed Floquet stability analysis of the square cylinder wake and suggested the critical value of the Reynolds number, $Re = 162 \pm 12$, for the onset of this regime. The results of the present study are consistent with those due to Robichaux et al. (1999).

Results obtained in the present work have been organized as per the following sections:

1. Instantaneous flow field.
2. Time-averaged integral parameters.
3. Rms values of force fluctuations.
4. Comparison with a circular cylinder.
5. Sensitivity of the transition to grid refinement and the size of the domain.

4.1. Instantaneous flow field

The flow past a square cylinder at low Reynolds numbers is characterized by the formation of a wake of staggered array of vortices. Laminar two-dimensional shedding without any spanwise instability has been observed up to a Reynolds number of 150. With an increase in the Reynolds number to 175, the wake of the square cylinder becomes structurally complex. In addition to the primary spanwise Kármán vortices (ω_z), secondary vortices are also generated in the wake. The secondary vortices can be viewed through two different view windows and they can be termed as the streamwise (ω_x) and transverse vortices (ω_y). Fig. 3(a) shows the instantaneous spanwise vortices on the mid-span ($z = 3.0$). The figure reveals the alternate staggered nature of the vortex street, thus signifying dominant periodicity in the flow. The streamwise wavelength of these spanwise vortices is about 6.2, though not a constant along the flow direction. Specifically, the near-wake wavelength is smaller as compared to the far-wake. The reason for this difference in wavelength is the higher convective speed of the vortices in the far-wake, the strong interaction between the vortices with opposite signs being absent.

The contours of secondary vortices ω_y are presented in Fig. 3(b). The vortices have been plotted on the mid-plane $y = 0$. The computations of the present study show that the spanwise wavelength (λ_z) of these vortices is about three and secondary instability is termed as Mode-A. Fig. 3(b) also shows the presence of the regular

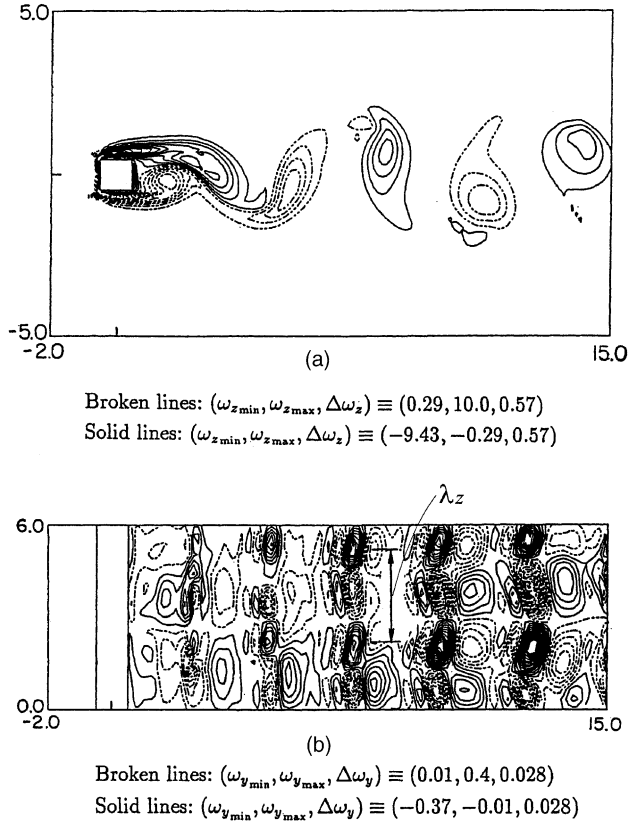

Fig. 3. Vorticity contours at a Reynolds number of 175: (a) spanwise vorticity and (b) transverse (secondary) vorticity on x–z mid-plane at $y = 0$. The secondary vortices show Mode-A pattern with a spanwise wavelength of three.

large-scale secondary vortices filling the span of the flow domain. At a Reynolds number of 150, the spanwise vorticity plots are similar to Fig. 3(a), but the transverse vorticity is zero everywhere. Thus, Fig. 3(b) is an indication of the flow becoming three-dimensional between Reynolds numbers of 150 and 175. Sohankar et al. (1999) have found that at $Re \leqslant 150$ the wake of a square cylinder is laminar, two-dimensional and characterized by the primary spanwise Kármán vortices. They have also concluded that the wake shows spanwise secondary instability and becomes three-dimensional in the range between $Re = 150$ and 200.

Fig. 4(a) shows the spanwise vorticity contours at the spanwise mid-plane for a Reynolds number of 250. The vortices in Fig. 4(a) are structurally complex as compared to Mode-A, Fig. 3(a). The wavelength of this component of vorticity is about 6.9 which is larger than 6.2, the corresponding wavelength of Mode-A. The contours of transverse vorticity on the mid-plane ($y = 0$) are presented in Fig. 4(b) at the Reynolds number of 250. The spanwise wavelength of these vortices is in the range 1.2–1.4 being smaller than $\lambda_z \simeq 3$ for Mode-A and this is called Mode-B secondary instability.

4.1.1. Vortex dislocation

A closer examination of the flow field at a Reynolds number of 175 shows that the vortex dislocation phenomenon reported by Williamson (1992) for a circular cylinder is also present for the square cylinder. As mentioned earlier, vortex dislocation is the intermittent low-frequency modulation due to the formation of a large-scale irregularity in the near-wake. It may be mentioned that vortex dislocation is generated between the spanwise cells due to the out-of-phase movement of the primary vortex in each cell. Following Williamson (1992), two types of vortex dislocations can be identified. In one, a rather twisted web of vortex linking occurs across the cell boundaries. Such a dislocation is one-sided and lacks symmetry. A two-sided dislocation occurs due to the local phase variation within larger cells of the shed vortices in association with the parallel shedding. The symmetry of the dislocation about the mid-span is a proof that the dislocated vortices are two-sided. Here, dislocation in the spanwise direction undergoes symmetric spreading.

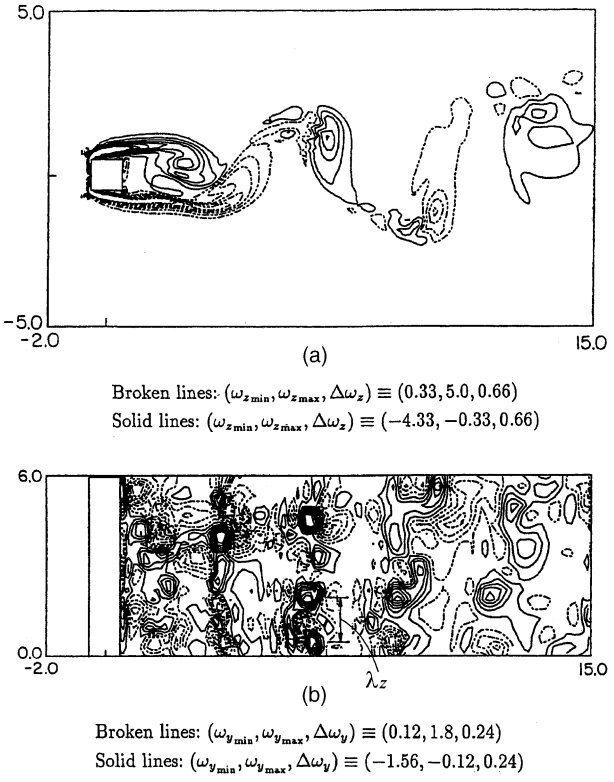

Fig. 4. Vorticity contours and iso-surfaces at a Reynolds number of 250: (a) spanwise vorticity contours (b) transverse (secondary) vorticity contours on x–z mid-plane at $y = 0$.

However, the natural vortex dislocation may appear randomly in space as well as in time. Fig. 5(a) shows the spanwise vorticity at the mid-span at the instant when the flow suffers vortex dislocation. The formation of vortex dislocation is understood from Fig. 5(b) where the transverse vorticity on the mid-plane ($y = 0$) is shown. Though originating in the near-wake, Fig. 5(b) shows the dislocation to be present a considerable distance downstream of the cylinder. The evolution of the dislocation shown later in Fig. 6 reveals that the dislocation is convected downstream after its formation in the near wake. The similar behavior of the transverse vorticity has been observed by Sohankar et al. (1999) at $t = 329$.

The dislocation in Fig. 5(b) shows that the spreading is two-sided with the frequency and phase of shedding on either side of the dislocation being equal. The two-sided dislocation forms a Λ structure, evident in Fig. 5(b). The Λ structure is seen far downstream, just before the outflow plane, in Fig. 5(b). Such structures have been documented by Williamson (1992). In contrast, the out-of-phase two-sided dislocation gives zig-zag symmetry about the cells of dislocation due to shift in either frequency or phase. In a two-sided dislocation, the vorticity concentration and vorticity cancellation can be discerned in Fig. 5(b) due to alternate in-phase and out-of-phase secondary vorticity distribution along the streamwise direction of the flow. To show the symmetry of the two-sided dislocation, two other spanwise vorticity contours have been presented in Fig. 5(c) ($z = 1.5$) and (d) ($z = 4.5$) for the same instantaneous flow field as in Fig. 5(a). Both the figures showing an identical trend in vortex shedding signifies that the dislocation is truly symmetric and two-sided. The vortex formation length at these two spanwise locations are similar as in Mode-A.

Fig. 6 shows the temporal evolution of the dislocation through the vorticity contours at a Reynolds number of

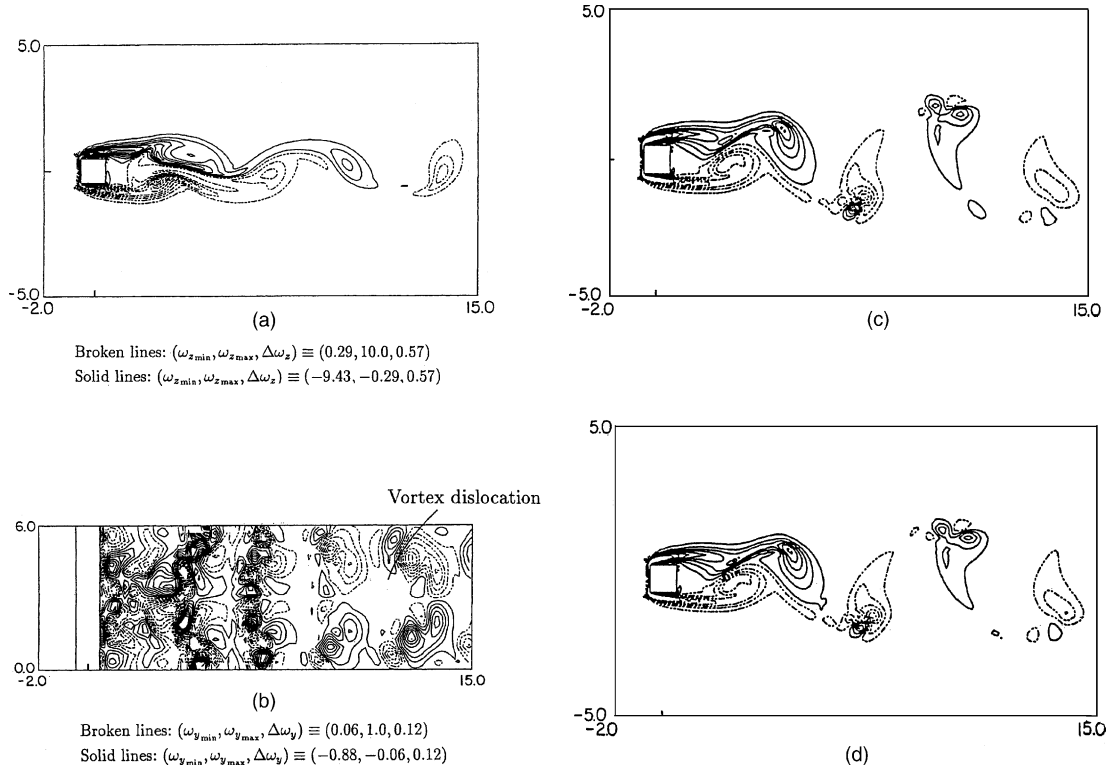

Fig. 5. Vorticity contours at a Reynolds number of 175 when vortex dislocation co-exists with regular shedding: (a) spanwise vorticity at mid-span ($z = 3.0$) (b) transverse (secondary) vorticity (c) spanwise vorticity at $z = 1.5$ and (d) spanwise vorticity at $z = 4.5$. The secondary vortices in (b) show the evidence of vortex dislocation shown by an arrow. The figure has been taken when the dislocation propagated in the far-wake. The specific time for this figure is $t = 412.25$.

175. In this figure, the contours at different times have been plotted on the same scale with identical maximum–minimum values of vorticity. The instantaneous drag-coefficient corresponding to Fig. 6 as a function of time is shown in Fig. 7. The time instances corresponding to the snapshots of Fig. 6 have been marked over the drag-coefficient signal. Fig. 6(a) corresponds to an instance when the vortex dislocation has already been initiated. Fig. 6(c) confirms that the spanwise spreading rate of the dislocation is high in the downstream direction. The increased spreading rate with increasing downstream distance is clear due to the fact the distances between the centers of the secondary vortices from the mid-span increases with the downstream distance. Fig. 6(d) and (e) show that the dislocation process gradually comes to a stop, in the sense that the near-wake is filled by three-dimensional secondary vortices. Thus, unlike the continuous shedding phenomenon, dislocation progress intermittently in time.

Dislocation may originate due to different reasons. Williamson (1992) has demonstrated experimentally the formation of dislocation by forcing a frequency discontinuity with the help of a disc having a diameter larger than the circular cylinder, and these dislocations were also found in natural transition experiments shown in Williamson (1992). The formation of a dislocation as a consequence of oblique shedding has also been demonstrated in these experiments. The present study did not employ any external forcing and vortex dislocation was possibly due to the phase variation within the large coherent structures. The other possibility is the merging of the secondary vortices in the spanwise direction. The regular shedding mode (Mode-A) shows a spanwise wavelength of secondary vortices to be 3B. The spanwise wavelength of the secondary vortices increases during the vortex dislocation by merging. This phenomenon is clear from the Fig. 6(a) where the secondary vortices show an increase in spanwise wavelength. This increase in the wavelength can be associated with a low frequency irregularity seen in vortex dislocation.

The results presented above show that subsequent to transition to three-dimensionality in the wake of a square cylinder, Mode-A appears together with the vortex dislocation process. The pattern can exist over a narrow Reynolds number range ($150 \leqslant Re \leqslant 175$). One can broadly expect that the Mode-A behavior is more probable in the vicinity of a Reynolds number of 150, while it is Mode-A with dislocations around a Reynolds number of 175. Transition in the wake of a square cylinder can now be characterized as follows: The flow is two-dimensional up to a Reynolds number of 150, and

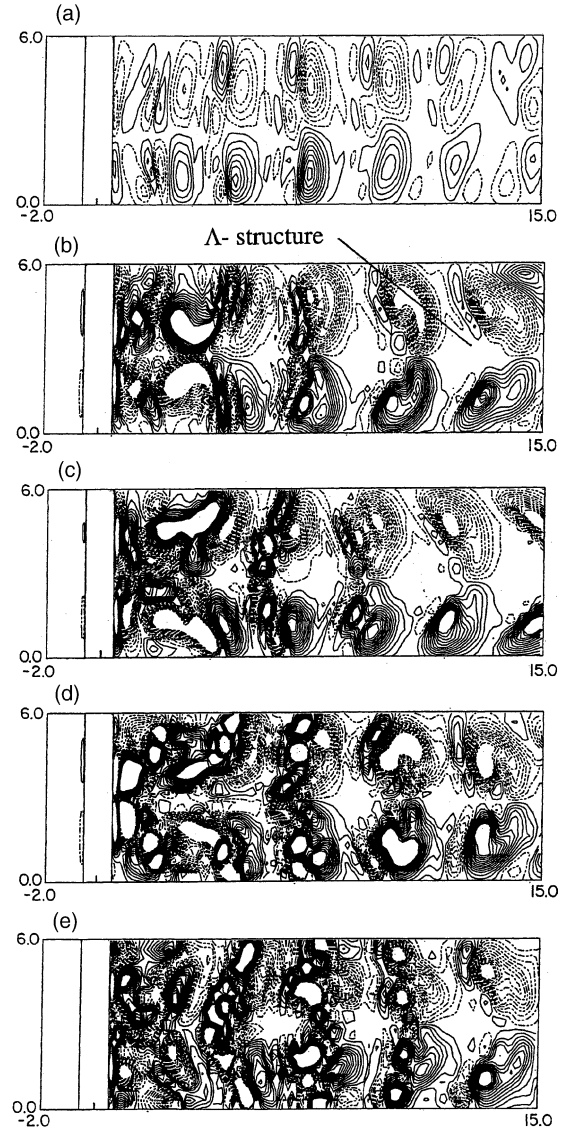

Fig. 6. Temporal evolution of vortex dislocation at various time t: (a) 510.11, (b) 541.99, (c) 553.81, (d) 561.59 and (e) 572.23 for a Reynolds number of 175.

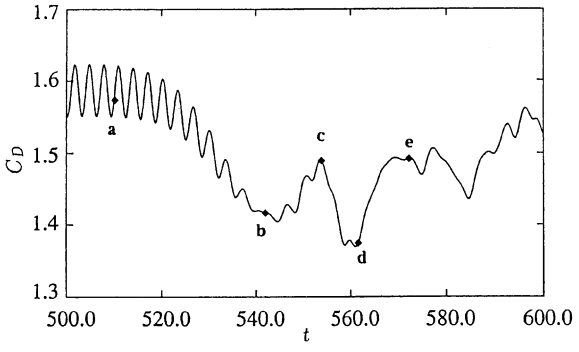

Fig. 7. Drag-coefficient signal showing the different instances of the vortex dislocation shown in Fig. 6.

becomes three-dimensional before $Re = 175$. The flow regime at about $Re = 175$ is also characterized by the presence of intermittent low frequency oscillations together with the three-dimensional shedding mode (Mode-A). There may exist a small range of Reynolds numbers beyond 150, in which the flow shows Mode-A behavior without any intermittent low-frequency, but this could not be detected in the present work. The sequence of transition to three-dimensionality is thus expected to be:

2D → Mode-A with dislocations → Mode-B(3D)

4.1.2. Comparison with the published literature

Sohankar et al. (1999) have reported results of a simulation of three-dimensional flow around a square cylinder in the Reynolds number range of 150 and 500 and for the aspect ratios of 6 and 10. The major findings of Sohankar et al. (1999) are the following. The transition of Mode-A type from two to three-dimensional shedding behind the square cylinder occurs in the Reynolds number range of 150–200. The spanwise wavelength of Mode-A is in the range of 2–5 cylinder widths. Beyond $Re = 250$, Mode-B dominates the wake with a corresponding spanwise wavelength of 1–1.5. Between $Re = 200$ and 250, the simulation shows the appearance of persistent low frequency force pulsations during the transient evolution and subsequently fades away at higher Reynolds numbers. The pulsations are seen in the spanwise-averaged forces. They can be classified into a high force (HF) phase and low force (LF) phase and roughly correspond to a strongly two- and three-dimensional vorticity fields. Specifically, the HF phase shows a good spanwise correlation of the streamwise vorticity, while the LF phase reveals a poor correlation. Beyond $Re = 250$ (and upto 500), the authors report a strengthening of Mode-B, dominant vortex shedding and general, global features that indicate a return to two-dimensionality.

The difference between a circular cylinder flow and a square cylinder flow has been mentioned by Sohankar et al. (1999) in connection with wake behavior at Reynolds numbers >250 (and upto 500). For a square cylinder, the increase in the vorticity contained in the secondary flow was substantial, a factor of six on certain planes. For a circular cylinder, Mode-B was seen to be the dominant pattern, the force pulsations were completely absent and the spanwise correlation of the lift force was much smaller (Henderson, 1997). This trend has been traced to the feedback mechanism from the secondary vortices of Mode-B with the flow separation process, that causes a movement of the point of separation and thus an overall reduction in the wake circulation. The strengthening of the streamwise vorticity for a square cylinder is thus to be derived from the fixed points of separation at the rear corners. It can also explain why the Strouhal number decreases and the time and span averaged drag-coefficients increase with Reynolds

Table 1
Comparison of critical Reynolds numbers for various transition modes due to present computation, Robichaux et al. (1999) and Sohankar et al. (1999)

Investigations	Critical *Re*		
	Mode-A	Mode-B	Mode-S
Sohankar et al. (1999)	150–200	$\geqslant 250$	
Robichaux et al. (1999)	162 ± 12	190 ± 14	200 ± 5
Present investigation	150–175	$\geqslant 240$	

number for a square cylinder, while the opposite behavior is observed for a circular cylinder.

Table 1 compares the critical Reynolds numbers for different transitions found out by different researchers. Though the study of Sohankar et al. (1999) shows the evidence of pulsation at a relatively higher *Re* ($\geqslant 200$), there is no explicit reference to vortex dislocation. The study of Robichaux et al. (1999) does not reveal any pulsation in the flow field, neither do they encounter the vortex dislocation phenomenon. The present study gives conclusive evidence of the creation of the large scale structure and its effect on the dynamical behavior of the flow. The frequency of pulsation observed in the present study corresponds to 10–12 shedding periods whereas Sohankar et al. (1999) have found the frequency of pulsation to be equivalent to 10–16 shedding periods. Thus the present study confirms the findings of earlier investigations but establishes vortex dislocation as the physical phenomenon central to flow behavior at transitional Reynolds numbers. It has been found in the present study that the fluctuations start decreasing beyond $Re = 250$. Henderson (1997) has observed a similar behavior of the flow structure for a circular cylinder and has explained it as the following. The growth of Mode-B causes a large reduction in amplitude of Mode-A, driving the system back towards a two-dimensional state.

4.1.3. Instantaneous signals

To establish the differences between the modes of vortex shedding, the signal traces of the relevant quantities have been compared below. Fig. 8 shows the time traces of the transverse component of velocity at Reynolds numbers of 150 and 175 in the near-wake ($x = 1.23$) along the centerline. The dimensionless spectra of the signals shown in Fig. 8 were also calculated. The spectrum at a $Re = 175$ was found to be broader due to the presence of dislocation. However, the spectrum at $Re = 150$ shows only one peak corresponding to the primary shedding frequency. The frequency of vortex shedding in Mode-A with dislocations, is smaller due to the presence of the low frequency irregularity of vortex dislocation. If the dislocation from the flow field at $Re = 175$ is assumed to be absent at $Re = 175$ (which can be thought of Mode-A alone), the signal would have

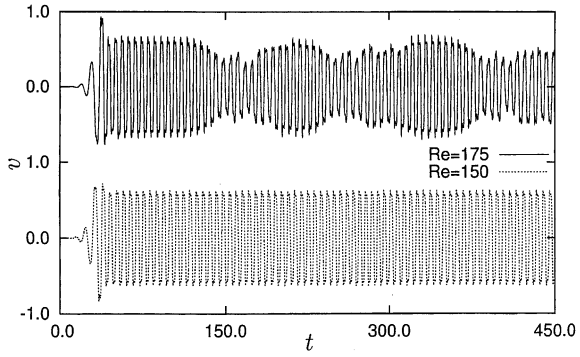

Fig. 8. Time traces of transverse velocity at two different Reynolds numbers. The time signal at a Reynolds number shows the evidence of low frequency intermittent irregularities.

given a frequency higher than the Mode-A with dislocations but is equal to the regular shedding frequency at $Re = 150$.

The variation of the instantaneous drag and lift coefficients with time are shown for a Reynolds number of 150 in Fig. 9(a). At a Reynolds number of 175, the force components exhibit a clear pulsation (Fig. 9(b)). A distinct and intermittent switching of the flow field is clear in this figure. There is a low frequency modulation (marked LD, low drag) in the time-series with the usual shedding mode (marked HD, high drag). The unusual intermittent low frequency modulation can be related to the vortex dislocation. The time-period of the dislocation is approximately fifteen times that of vortex shedding and the duration for which dislocation persists is about 10–12 times the shedding period. The decrease in the drag-coefficient during the period of vortex dislocation is due to a longer recirculation length (see Fig. 5(a)) compared to the regular shedding mode. Similarly the decrease in lift coefficient during the vortex dislocation period is also due to a reduced pressure drop across the transverse faces of the cylinder, again owing to a longer recirculation length. In the usual shedding mode there is an increase in the rms values of both the coefficients with Reynolds number. The rms fluctuations momentarily fall during vortex dislocation. With further increase in Reynolds number, the intermittent low frequency modulation in the flow decreases, and the pulsation phenomenon fades out, see Fig. 9(c), $Re = 290$.

4.2. Time-averaged integral parameters

The present section is concerned with the consequences of vortex dislocation on the time-averaged quantities. Fig. 10 is a comparison between the present two- and three-dimensional simulation with the computational results of Davis et al. (1984) and Franke et al. (1990), and the hotwire experiments of Okajima (1982). It may be mentioned that where there is an overlap of data (e.g., $Re = 100, 200$ and 250) the data points are

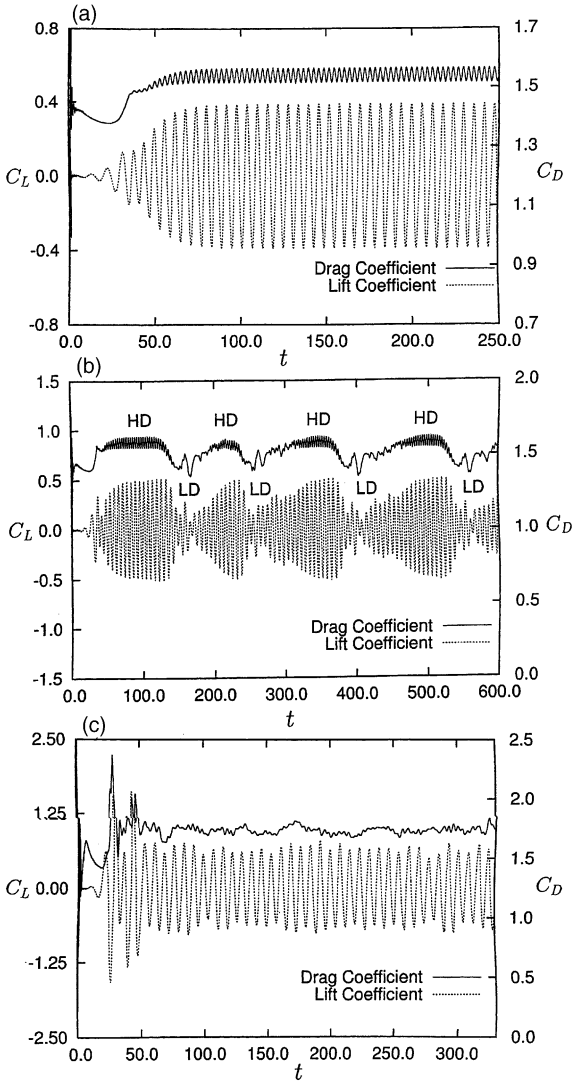

Fig. 9. Temporal variations of drag and lift coefficient at various Reynolds numbers: (a) $Re = 150$ (b) $Re = 175$ and (c) $Re = 290$.

offset for clarity. This figure shows that just beyond a Reynolds number of 175, the Strouhal number decreases. Beyond a Reynolds number of 250 for two-dimensional and 450 for three-dimensional calculations, there is an increase in Strouhal number. The reduction in the Strouhal number at a Reynolds number of 175 can be related to the formation of vortex dislocation. The experimental points of Okajima (1982) show significant scatter and preclude a precise investigation of this effect. The data points shown in Fig. 10 are averages determined from the reported experiments. The numerical simulation referred in Fig. 10 are two-dimensional in nature and also fail to capture this trend. Specifically at a Reynolds number of 175, the computed value of the Strouhal number is 0.158, when dislocation co-exists with the regular shedding mode and is lower than the value without dislocation ($=0.163$). A Strouhal number of 0.163 is also obtained at a Reynolds number of 150

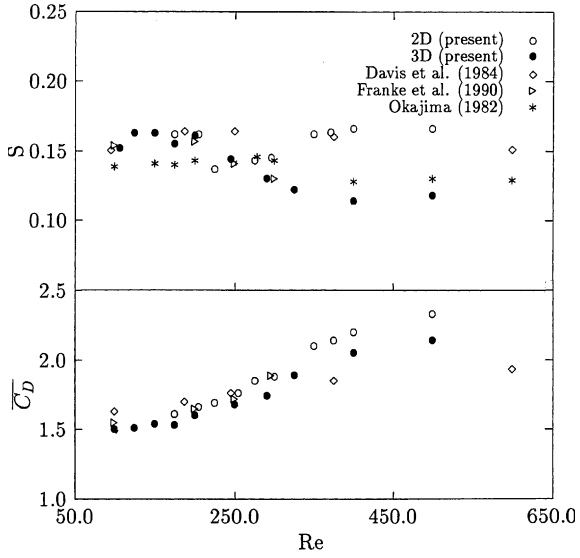

Fig. 10. Variation of Strouhal number and drag-coefficient with Reynolds number.

when the transition to three-dimensionality has not occurred. The Strouhal number increases to 0.161 at a Reynolds number of 200 when the dislocation largely fades away at this Reynolds number.

The variation of the time-averaged drag-coefficient, $\overline{C}_{\mathrm{D}}$ with Reynolds number is also shown in Fig. 10. The present three-dimensional computation shows a close association between the drag-coefficient and the Strouhal number. The inverse of the Strouhal number correlates with the time-averaged drag-coefficient over the entire range of Reynolds number. The time-averaged lift coefficient, $\overline{C}_{\mathrm{L}}$ was found to be less than 10^{-3} at all the Reynolds number studied. It has been observed that the results due to the present computation match quite well with Robichaux et al. (1999). The Strouhal number and the the average drag-coefficient due to Robichaux et al. (1999) are 0.157 and 1.64 at a Reynolds number of 200. The corresponding values due to the present computation are 0.163 and 1.67 respectively.

4.3. Rms values of force fluctuations

The rms values of the lift and drag-coefficients as a function of Reynolds number are presented in Table 2. There is a steady increase in the rms values upto a Reynolds number of 150. At a Reynolds number of 175, an increase in the rms value of drag-coefficient and a simultaneous decrease in that of lift coefficient are seen. This behavior can also be traced to vortex dislocation. During this process, the elongation of the shear layer leads to a lower value of the instantaneous drag-coefficient. Thus the rms value is higher though the time-averaged value is unaffected. The drop in the rms value of the lift coefficient can be explained by the lower

Table 2
Rms values of lift and drag-coefficients

Re	C'_L	C'_D
100	0.122	0.003
125	0.223	0.011
150	0.274	0.017
175	0.268	0.062
200	0.305	0.026
250	0.150	0.032
290	0.473	0.033

transverse velocity fluctuations (Fig. 8) experienced by the cylinder during vortex dislocation. A second discontinuity is observed at a Reynolds number of 250. This can be attributed to the switching of the flow from Mode-A (or Mode-A with dislocations) to Mode-B. Mode-B contains fine-scale structures when compared to Mode-A. These small-scales also lead to smaller transverse fluctuations. The higher rms value of the drag-coefficient is a consequence of the higher pressure drop across the cylinder in the streamwise direction due to the formation of small-scale structures. The rms values of the lift and drag-coefficient subsequently show a steady increase with increasing Reynolds number. At a Reynolds number of 325, C'_L and C'_D were found to be 1.015 and 0.113 respectively. A possible explanation is the resonance due to interaction between the shear layer and Kármán frequencies. It can also be seen that the force fluctuations have more influence on lift (via the fluctuating component C'_L), which is consistent with the results of circular cylinder.

4.4. Comparison with a circular cylinder

The transition phenomena in a bluff body wake particularly for a circular cylinder have been studied extensively in the past. Though the macroscopic flow past a square cylinder resembles that of circular cylinder, there are major differences as far as the separation mechanism and the related integral parameters such as Strouhal number, lift and drag-coefficient are concerned. In this context, it is surprising to note that there is similarity between the circular and square cylinders in their transition sequence at low Reynolds numbers. In the case of a square cylinder, the separation points are fixed at the front leading edges. In the case of a circular cylinder the separation points vary with Reynolds number. The after-body of a square cylinder, which is equal to the width of the cylinder, extends into the wake. In the case of a circular cylinder, the after-body which extends into the wake is of the order of half a diameter. Also, the flat after-body of the square cylinder brings about a stabilizing effect to the separated shear layers. These differences influence the transition process to three-dimensionality.

The flow past a circular cylinder experiences a transition to three-dimensionality at a Reynolds number of 180 (Williamson, 1996a). The Floquet stability analysis carried out by Henderson and Barkley (1996) shows that the critical Reynolds number corresponding to three-dimensionality is 188.5. The present study shows the critical Reynolds number to fall in the range of 150–175 for a square cylinder.

The wake of a circular cylinder undergoes a series of transition with respect to the formation of the secondary spatial structures having different spanwise wavelengths. The transition to three-dimensionality is sensitive to various factors such as upstream conditions and end conditions of the cylinder. Williamson (1996b) has reported a spanwise wavelength of 3.0–4.0 at a Reynolds number of 189–194 for Mode-A and 1.0 at a Reynolds number of 250 for Mode-B for flow past a circular cylinder. Numerical calculation and experiments of Zhang et al. (1995) have shown that the wavelengths are 4 for Mode-A and 1 for Mode-B at Reynolds numbers of 200 and 240 respectively. Henderson (1997) has found that Mode-A is triggered at a Reynolds number of 195 and the corresponding wavelength is 3.96. This study also shows that the wake of the cylinder has a Mode-B pattern at a Reynolds number of 265 with a spanwise wavelength of 0.822. Brede et al. (1996) have reported Mode-A at a Reynolds number range of 160–240 for flow past a circular cylinder and the corresponding wavelength is 4.5. At a Reynolds number >240 the pattern was found to be Mode-B with a spanwise wavelength of 1. The spanwise wavelength in the present study has been found to be 3 for Mode-A and the corresponding Reynolds number is 175. Mode-B does not have a constant spanwise wavelength but falls in the range of 1.2–1.4 at a Reynolds number of 250. The wake vorticity structures of the present simulation are quite consistent with the observations of Sohankar et al. (1999).

In the present study, the instantaneous contours of the secondary vortices (ω_y) in Mode-A have been found to be of alternate sign along the cylinder axis (Fig. 3(b)). These contours are similar to those observed by Zhang et al. (1995) for a circular cylinder. The structures of secondary vortices in Mode-B of the present study (Fig. 4(b)) are also similar to those of Zhang et al. (1995).

The wake of the square cylinder experiences intermittent low frequency pulsation at definite Reynolds numbers. This phenomenon has been attributed to the formation of large-scale irregularities, namely vortex dislocation. Williamson (1992) has observed low frequency fluctuations in an extensive set of experiments. This is corroborated from the Fig. 4 of Williamson (1992) which contains the downstream decay of streamwise fluctuations at a Reynolds number of 183. The contours of the secondary vortices of the present study clearly show the formation of dislocation at the mid-span. An

important characteristic of a dislocation is its high spanwise spreading rate. Fig. 5(b) of Williamson (1992) shows this phenomenon and is remarkably similar to Fig. 6(c) of the present study.

The transition sequence to three-dimensionality envisaged by Williamson (1996c) for a circular cylinder was $2D \rightarrow A \rightarrow A(\text{with dislocations}) \rightarrow B$. A subsequent review by the same author (Williamson, 1997), indicated that it is seldom possible to distinguish between Mode-A (without dislocations) and Mode-A (with dislocation). However, the present study confirms the scenario of Williamson (1997) and shows that this particular sequence for a square cylinder to be $2D \rightarrow A(\text{with dislocations}) \rightarrow B$.

4.5. Sensitivity of the transition to grid refinement and the size of the domain

The transition to three-dimensionality and vortex dislocation may arise due to disturbances caused by the grid, domain size and end conditions (Sohankar et al., 1999). In the present study, attempts have been made to see the differences in the evolution of vortex dislocation and to ensure that the dislocation is a physical phenomenon and does not occur due to the numerical errors in discretization and due to the smaller domain size. Studies have also been carried out to investigate the differences in the vortex structures with a higher aspect ratio (A/B) and the evolution of dislocation with respect to the aspect ratio and Reynolds number.

The sensitivity of the instantaneous flow field to the grid has been studied using three different grid sizes, namely $178 \times 80 \times 22$, $178 \times 80 \times 42$ and $218 \times 104 \times 22$. Fig. 11 shows the vorticity contours which reveal the phenomenon of vortex dislocation at a Reynolds number of 175 for a mesh of size of $178 \times 80 \times 42$. The spanwise vorticity contours, illustrated in Fig. 11(a) reveal a structures similar to Fig. 5(a). The vortex dislocation is clear from the Fig. 11(b) and is similar to the Fig. 6(b) and (c). The global quantities, such as the Strouhal number, mean and rms values of drag and lift reveal negligible variation with grid size (see Table 3). Therefore, the vortex dislocation process in the present study is not an artifice of grid size and it appears to be a physical phenomenon.

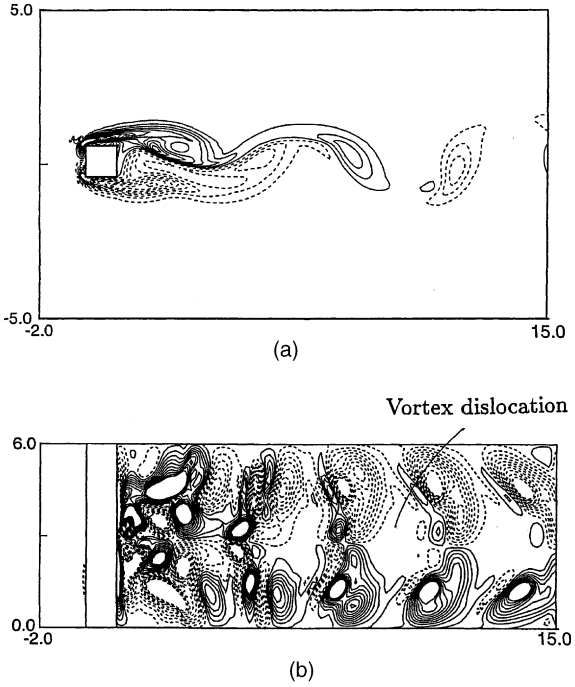

Fig. 11. (a) Spanwise and (b) transverse (secondary) vorticity contours at a Reynolds number of 175 and $A/B = 6.0$ and $178 \times 80 \times 42$ grid mesh. The figure shows the existence of vortex dislocation.

To study the effect of the domain size on transition, the aspect ratio A/B was increased from 6 to 10 units along with a proportionally higher number of computational cells. The dislocation process at $Re = 175$ was found to be quite weak. However, at a Reynolds number of 195, the entire sequence of events characterizing vortex dislocation was reproduced (Fig. 12(a) and (b)). The relative comparison between the size of this large-scale structure and the domain size is clearly discerned in this figure. For higher A/B, two vortex dislocation units are seen to propagate in the wake. This suggests that the dimensionless length scale of vortex dislocation is around 5.0 widths. The distribution of transverse vorticity on the vertical mid-plane (Fig. 12(b)) reveals that the size of the large-scale structure obtained in this

Table 3
Grid independence test

Re	Grid size	S	$\overline{C_D}$	$\overline{C_L}$	C'_D	C'_L
175	$178 \times 80 \times 22$	0.158	1.53	0.0003	0.062	0.268
	$178 \times 80 \times 42$	0.159	1.52	−0.0006	0.061	0.260
	$218 \times 104 \times 22$	0.159	1.54	0.0003	0.064	0.269
250	$178 \times 80 \times 22$	0.147	1.69	0.0002	0.032	0.145
	$178 \times 80 \times 32$	0.154	1.69	0.003	0.033	0.193
	$218 \times 104 \times 22$	0.150	1.72	0.003	0.044	0.183
500	$178 \times 80 \times 32$	0.120	2.14	−0.005	0.193	1.442
	$218 \times 104 \times 32$	0.116	2.17	0.005	0.205	1.454

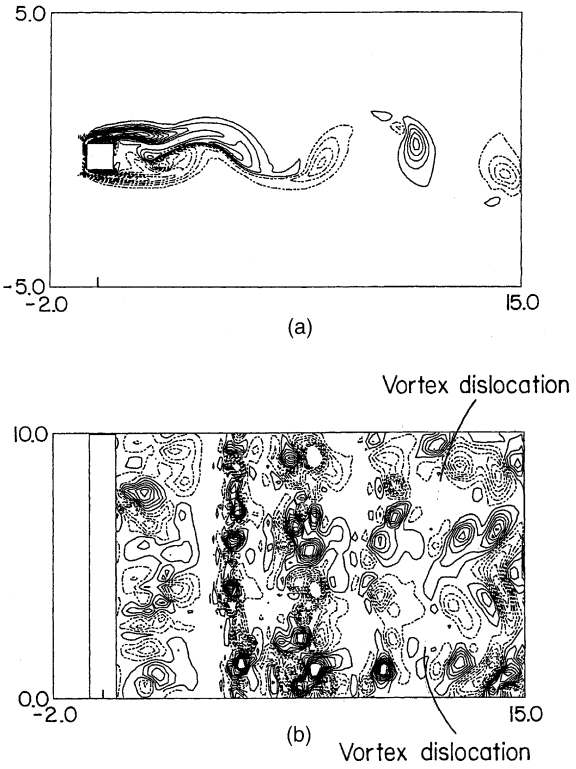

Fig. 12. Vorticity contours at a Reynolds number of 195 and $A/B = 10.0$. The vortex dislocation co-exists with regular shedding: (a) spanwise vorticity at the mid-span ($z = 5.0$) (b) transverse (secondary) vorticity. The secondary vortices in (b) show the evidence of two vortex dislocations.

investigation is smaller than that of the domain size and the vortex dislocation is a physical phenomenon. It is worth mentioning that the spanwise wavelengths associated with Mode-A instability for the case with Reynolds number of 195 and $A/B = 10$ and the case with $Re = 175$ and $A/B = 6$ are equal. Also to be mentioned is that Sohankar et al. (1999) have used a spanwise length of six in their DNS calculations. However, they have simulated the flow with a spanwise length of 10 as well for $Re = 200$ and 250. They observed negligible effect of spanwise length on the global parameters, such as the dominant wake frequency, mean and rms values of lift and drag. Sohankar et al. (1999) have also found that the pulsation due to spanwise length of six occurs more frequently with stronger amplitude than that due to spanwise length of 10. The main conclusion to emerge here is that the domain size fixes the transition Reynolds number but not the physical description of the events following the transition.

5. Conclusions

A numerical study of three-dimensional flow past a square cylinder in the Reynolds number range of 150–500 has been reported. The flow is seen to be predominantly two-dimensional at a Reynolds number of 150. At about a Reynolds number of 175, the flow is three-dimensional, with Mode-A instability. In Mode-A, a three-dimensional structure with a spanwise wavelength of three is formed. In Mode-A with dislocations, this is accompanied by intermittent large-scale irregularities identified as vortex dislocation. The time for which vortex dislocation persists is 10–12 times the shedding period. While Mode-A is realizable closer to a Reynolds number of 150, the appearance of Mode-A with dislocations is most likely closer to a Reynolds number of 175. At all Reynolds numbers, the flow is shedding dominated, and hence by the spanwise vortices, three-dimensionality being superimposed on this flow field.

In summary, the numerical results of the present work show that:

1. Transition to three-dimensionality occurs at a Reynolds number between 150 and 175.
2. Flow around a Reynolds number of 175 shows Mode-A instability together with intermittent low frequency irregularities, known as vortex dislocations.
3. Vortex dislocation possibly occurs as a result of vortex merging in the spanwise direction or due to phase variation within the large coherent structures.
4. Flow at a Reynolds number of 250 reveals Mode-B having a finer-scale compared to Mode-A.
5. The spanwise wavelengths corresponding to Mode-A and Mode-B are 3 and 1.2–1.4 respectively.
6. The change in grid size and the domain size do not change the dislocation and thus dislocation is a physical phenomenon.
7. The results for the square cylinder are in good accordance with the three-dimensional modes of transition that are well-known in the circular cylinder wake.

Acknowledgements

The research was supported by the ARDB grant RD/134/100/10/1032. The authors are grateful to the unknown referees for the valuable comments.

References

Brede, M., Eckelmann, H., Rockwell, D., 1996. On secondary vortices in the cylinder wake. Phys. Fluids 8, 2117–2124.

Davis, R.W., Moore, E.F., Purtell, L.P., 1984. A numerical-experimental study on confined flow around rectangular cylinders. Phys. Fluids 23, 46–59.

Franke, R., Rodi, W., Schönung, B., 1990. Numerical calculation of laminar vortex-shedding flow past cylinders. J. Wind Eng. Ind. Aero. 35, 237–257.

Harlow, F.H., Welch, J.E., 1965. Numerical calculation of time-dependent viscous incompressible flow of fluid with free surfaces. Phys. Fluids 8, 2182–2188.

Henderson, R.D., 1997. Nonlinear dynamics and pattern formation in turbulent wake transition. J. Fluid Mech. 352, 65–112.

Henderson, R.D., Barkley, D., 1996. Secondary instability in the wake of a circular cylinder. Phys. Fluids 8, 1683–1685.

Hoffman, G., Benocci, C., 1994. Numerical simulation of spatially-developing planer jets, AGARD, CP-551, pp. 26.1–26.6.

Mittal, R., Balachandar, S., 1995. Generation of streamwise vortical structures in bluff-body wakes. Phys. Rev. Lett. 75, 1300–1303.

Okajima, A., 1982. Strouhal numbers of rectangular cylinders. J. Fluid Mech. 123, 379–398.

Orlanski, I., 1976. A simple boundary condition for unbounded flows. J. Compt. Phys. 21, 251–269.

Robichaux, J., Balachandar, S., Vanka, S.P., 1999. Three-dimensional Floquet instability of the wake of square cylinder. Phys. Fluids 11, 560–578.

Saha, A.K., 1999. Dynamical characteristics of of the wake of a square cylinder at low and high Reynolds numbers. PhD Thesis, Indian Institute of Technology Kanpur, India.

Saha, A.K., Muralidhar, K., Biswas, G., 2000a. Numerical simulation of transition and chaos in two-dimensional flow past a square cylinder. ASCE J. Engg. Mechanics 126, 523–532.

Saha, A.K., Muralidhar, K., Biswas, G., 2000b. Vortex structures and kinetic energy budget in two-dimensional flow past a square cylinder. Comput. Fluids 29, 669–694.

Sohankar, A., Norberg, C., Davidson, L., 1999. Simulation of three-dimensional flow around a square cylinder at moderate Reynolds numbers. Phys. Fluids 11, 288–306.

Tombazis, N., Bearman, P.W., 1997. A study of three-dimensional aspects of vortex shedding from a bluff body with a mild geometric disturbance. J. Fluid Mech. 330, 85–112.

Williamson, C.H.K., 1989. Oblique and parallel modes of vortex shedding in the wake of a circular cylinder at low Reynolds numbers. J. Fluid Mech. 206, 579–627.

Williamson, C.H.K., 1992. The natural and forced formation of spot-like 'vortex-dislocations' in the transition of a wake. J. Fluid Mech. 243, 393–441.

Williamson, C.H.K., 1996a. Vortex dynamics in the cylinder wake. Ann. Rev. Fluid Mech. 28, 477–539.

Williamson, C.H.K., 1996b. Mode-A secondary instability in wake transition. Phys. Fluids 8, 1680–1682.

Williamson, C.H.K., 1996c. Three-dimensional wake transition. J. Fluid Mech. 328, 345–407.

Williamson, C.H.K., 1997. Advances in our understanding of vortex dynamics in bluff body wakes. J. Wind Engr. Indust. Aero. 71, 3–32.

Zhang, H., Fey, U., Noack, U., König, M., Eckelmann, H., 1995. On the transition of the cylinder wake. Phys. Fluids 7, 779–794.